Prepared for submission to JINST

Machine Learning Optimization of BEGe Detector Event Selection in the VIP Experiment

S. Manti[1,*,†] **S.H. Yip**[2,†] **M. Bazzi**[1] **N. Bortolotti**[1,3] **M. Bragadireanu**[4] **M. Cargnelli**[5,6] **I. Carnevali**[1] **A. Clozza**[1] **L. De Paolis**[1] **R. Del Grande**[7,1] **C. Guaraldo**[1,‡] **M. Iliescu**[1] **M. Laubenstein**[8] **J. Marton**[5,6] **F. Napolitano**[9,10] **F. Nola**[1] **K. Pischicchia**[1,3] **A. Porcelli**[11,12] **A. Scordo**[1] **F. Sgaramella**[1] **D. Sirghi**[3,1,4] **F. Sirghi**[1,4] **J. Zmeskal**[5,‡] **C. Curceanu**[1,4]

[1] *Laboratori Nazionali di Frascati INFN, Frascati, Italy*
[2] *University of California, Berkeley, CA 94720, USA*
[3] *Centro Ricerche Enrico Fermi, Museo Storico della Fisica e Centro Studi e Ricerche "Enrico Fermi", Roma, Italy*
[4] *IFIN-HH, Institutul National pentru Fizica si Inginerie Nucleara Horia Hulubei, 30 Reactorului, 077125, Magurele, Romania*
[5] *Stefan Meyer Institute for Subatomic Physics, Vienna, Austria*
[6] *Atominstitut, Technische Universität Wien, Stadionallee 2, 1020 Vienna, Austria*
[7] *Faculty of Nuclear Sciences and Physical Engineering, Czech Technical University in Prague, Břehová 7, 115 19, Prague, Czech Republic*
[8] *Laboratori Nazionali del Gran Sasso, Istituto Nazionale di Fisica Nucleare, Via G. Acitelli 22, 67100, Assergi, Italy*
[9] *Via A. Pascoli 06123, Perugia (PG), Italy, Dipartimento di Fisica e Geologia, Università degli studi di Perugia*
[10] *INFN Sezione di Perugia, Via A. Pascoli, 06123 Perugia, Italia*
[11] *Centro de Investigacíon, Tecnología, Educacíon y Vinculacíon Astronómica, Universidad de Antofagasta, Avenida Angamos 601, 1240000, Antofagasta, Chile*
[12] *Faculty of Physics, Astronomy, and Applied Computer Science, Jagiellonian University, Kraków, Poland*
[*] *Corresponding Authors*
[†] *These authors contributed equally*
[‡] *Deceased*

E-mail: simone.manti@lnf.infn.it, jason17@berkeley.edu

Abstract: Experiments that test the foundations of quantum mechanics, such as possible violations of the Pauli Exclusion Principle or spontaneous wave-function collapse, require detectors with high sensitivity and very low background noise. The VIP-2 experiment at the Gran Sasso National Laboratory operates in such a low-background environment, using a Broad-Energy Germanium (BEGe) detector to measure background radiation and set limits on collapse models in the low-energy range. Here we report recent work on improving the data acquisition system to detect low-energy events. Our approach uses a denoising autoencoder followed by a classifier applied to its output to clean waveform data and identify valid events. The denoising autoencoder enables feature-based selection of good events, improving noise suppression and event quality. The method was validated on data acquired in 2021, consisting of more than 20,000 waveforms. The classifier achieved an AUC of 0.99 and an accuracy of 95%. These improvements lower the effective energy threshold to 10 keV and increase both resolution and signal-to-background ratio for the characteristic Pb and Bi peaks. The peak resolution reached 1 keV at 100 keV, and the signal-to-background ratio improved by 20%. This development enables more precise and sensitive searches for rare quantum phenomena at low energies.

Keywords: VIP, BEGe, Machine Learning

ArXiv ePrint: 1234.56789

Contents

1 Introduction 1

2 BEGe Event Selection Strategy 2

3 Results and Discussion 6

4 Conclusions 7

1 Introduction

Experimental tests of the foundations of quantum mechanics require extreme sensitivity, as they target phenomena that, if observed, would occur at very reduced rates. Such rare-event searches provide a unique window into possible deviations from the standard quantum framework, complementing more conventional precision tests and opening opportunities to probe new physics at the interface between microscopic and macroscopic scales [1, 2].

Among the most fundamental principles of quantum theory is the Pauli Exclusion Principle (PEP) [3], which underlies the structure of atoms, the stability of matter [4], and even the behavior of astrophysical objects like neutron stars [5]. Its validity is directly linked to the Spin–Statistics Theorem [6], which dictates that fermions (bosons) obey antisymmetric (symmetric) wave functions under exchange of particles. Any violation of PEP would have profound implications, pointing to physics beyond the established quantum framework. From an experimental point of view, such violations could manifest as examples of anomalous atomic transitions, shifted by a few tenths of a keV from the standard spectral lines [7]. Establishing increasingly stringent limits on such effects is therefore a central goal of dedicated rare-event searches.

Another direction involves models of spontaneous wave-function collapse, which attempt to resolve the measurement problem by introducing additional physical mechanisms that suppress quantum superpositions at macroscopic scales. Prominent examples include the Continuous Spontaneous Localization (CSL) model [8] and the Diósi–Penrose (DP) model [9, 10]. Both predict the spontaneous emission of radiation, in particular X-rays in the keV range, which can serve as experimental signatures of the particular collapse model especially in the low-energy regime [11].

Detecting such rare and subtle signatures requires not only excellent energy resolution but also extremely low background. Underground laboratories play a crucial role in this context. The Gran Sasso National Laboratory (LNGS) provides a uniquely low-background environment for the study of rare events. Located under approximately 1400 m of rock-equivalent to 3800 m w e water-equivalent (m w.e.), the overburden reduces the cosmic muon flux to only about $3.41 \times 10^{-4}\,\mathrm{m^{-2}\,s^{-1}}$ [12]. This substantial attenuation of the muon flux enables experiments at LNGS to achieve significantly reduced background levels. This makes LNGS one of the world's premier environments for rare-event searches, hosting experiments ranging from neutrino physics to dark matter and double beta decay [13–15].

Within this environment, the VIP (Violation of the Pauli Exclusion Principle) collaboration has progressively tightened the upper limits on PEP-violating events. The original VIP experiment set an upper limit of $\beta^2/2 < 4.7 \times 10^{-29}$ [16], the most stringent constraint at the time. Its successor, VIP-2, pushed this further, establishing limits of $\beta^2/2 \leq 6.8 \times 10^{-42}$ (Bayesian, 90% CL) and $\beta^2/2 \leq 7.1 \times 10^{-42}$ (Frequentist CL_s, 90% CL) [17]. The ongoing VIP-3 effort is extending the search across the periodic table, with high-Z targets such as zirconium, silver, palladium, and tin [18].

A central element of these experiments is the detector technology. Broad Energy Germanium (BEGe) detectors combine the features of coaxial and low-energy HPGe designs, covering a wide dynamic range from a few keV up to several MeV. They are particularly suited for rare-event searches because of their excellent resolution and efficiency at low energies. However, achieving thresholds of a few keV is challenging due to microphonic noise and electronic instabilities, which can obscure faint signals precisely in the energy range of interest for PEP-violating transitions and collapse-induced radiation [11]. ML for BEGe[A] In this work, we report recent advances in the operation of a BEGe detector within the VIP program at LNGS. Two key improvements were implemented. First, the detector setup was mechanically and acoustically isolated using a soundproof box and pneumatic suspension, suppressing microphonic contributions. Second, we developed and validated a machine–learning–based event selection strategy, employing a denoising autoencoder and a convolutional neural network to enhance discrimination between signal and background. These methods were applied to data acquired in 2021, demonstrating improved effective energy threshold and a higher signal-to-background ratio.

The remainder of this paper is organized as follows. Section 2 describes the experimental setup, including the BEGe detector and its isolation system. Section 3 introduces the machine-learning framework for event selection, with emphasis on the denoising and classification stages. Section 4 presents the performance validation with the 2021 dataset and discusses the improvements in resolution, threshold, and background rejection. Section 5 concludes with a summary and an outlook for future developments in the VIP program and related rare-event searches.

2 BEGe Event Selection Strategy

Event selection was performed using pulse shape analysis (PSA) on the acquired waveforms of the BEGe setup. To automate this selection and integrate it in the data acquisition, we employed deep learning with a Denoising Autoencoder (DAE) [19] with two main objectives. First, to remove noise from the waveforms and improve the selection of low-energy events. Second, to extract features that help in distinguishing normal events from anomalous ones (e.g. multi-site, saturated, and similar events). The latter is important for the creation of a dataset for supervised training of a classifier connected to the output of the DAE, allowing for anomaly detection of events.

This ML-aided PSA procedure was validated using the data collected in 2021 [11], which consist of more than 20000 events. For each event, a waveform is recorded by the BEGe detector electronics through a 400 MHz digitizer spanning 1024 samples, giving a total acquisition window of 2.55 μs. Further details on the BEGe apparatus are provided in our previous article [11]. We implemented the DAE within the Keras framework (v3.5.0). The DAE, which in input is operating on both the waveform and its derivative, is based on a one-dimensional (1D) convolutional neural network (CNN) with an encoding and decoding structure. The encoder comprises three convolutional layers with progressively decreasing filter sizes (i.e. 64, 32, 16), each followed by the rectified linear unit (ReLU) activation function, and max-pooling operations. The temporal dimension of the waveform in the input layer was reduced to 128 to decrease network complexity and shorten training time. The chosen input size and number of hidden layers represent a balance between model complexity, training efficiency, and the performance of both the DAE and the attached classifier. The decoder mirrors the encoder structure, using upsampling layers and additional convolutional layers with ReLU activation to restore the original waveform, followed by a final convolutional layer with linear activation to produce the reconstructed signal. The model is trained using the Adam optimizer with a learning rate of 10^{-4}. No hyperparameter tuning was required, since both the DAE and the CNN classifier achieved excellent performance with their initial configurations.

To train the DAE, we created a synthetic dataset of pulses that resemble the typical scenarios of events in our BEGe detector setup (see Figure 1). A normal event (see Figure 1a) corresponds to single-site energy depositions occurring within the bulk of the germanium detector, where the electric field is uniform and charge carriers are efficiently collected at the electrodes. These events are characterized by a prompt, steep

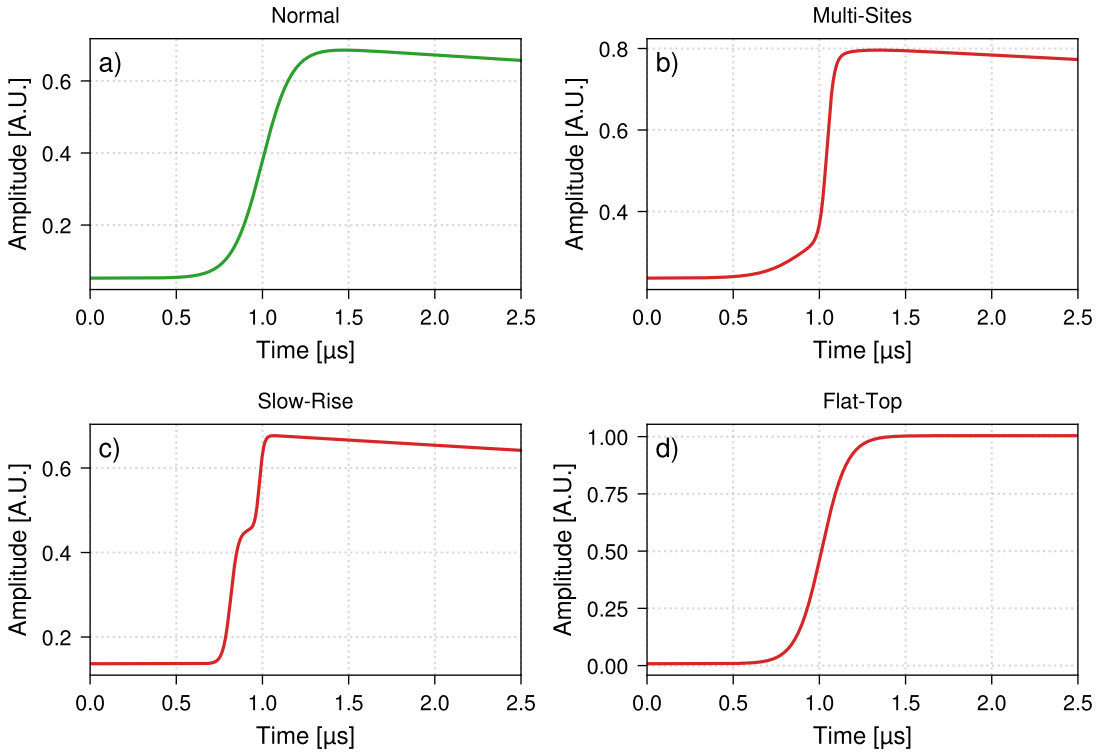

Figure 1: Examples of the four pulse types in the synthetic dataset used to train the Denoising Autoencoder: a normal pulse (green) in panel a, and anomalous pulses (red): multi-site (panel b), slow-rise (panel c), and saturated (panel d).

rising edge and an exponential decay, and represent the expected signal. Multi-site pulses (see Figure 1b) are generated to mimic the response to events in which energy is deposited at multiple, spatially separated locations within the detector volume. Such events can arise from, for example, Compton scattering or coincident background interactions. The resulting pulse shapes typically exhibit multiple rising steps or a more complex rise profile, reflecting the superposition of charge collection from each interaction site. Slow-rise pulses (see Figure 1c) are included to model interactions occurring near the detector surfaces, where the electric field strength is reduced. In these regions, charge carriers drift more slowly to the electrodes, resulting in a notably slower rise time compared to bulk events. The inclusion of slow-rise pulses in the training set allows the DAE to learn features associated with surface backgrounds, which can be subsequently suppressed through pulse shape discrimination, thereby improving the overall signal-to-noise ratio. Flat-top (see Figure 1d) are also incorporated in the dataset. These pulses are characterized by a rapid rise followed by a plateau, which can occur when the detector response saturates due to high-energy depositions or limitations in the readout electronics. Including flat-top pulses in the training set is crucial to ensure that the DAE can recognize and appropriately process saturated signals, which may otherwise be misidentified or improperly reconstructed. These categories follow the standard classification established in BEGe pulse shape analysis studies [20–22]. Each simulated pulse was superimposed with noise to reproduce the conditions of the experimental setup. Two noise components were considered: (i) white Gaussian noise, representing intrinsic electronic fluctuations, and (ii) colored noise generated by integrating a white noise process to emulate the low-frequency microphonic and environmental instabilities observed in the detector. The relative amplitude of the two components was tuned to match the baseline noise spectrum previously characterized for the BEGe setup

[11]. Two distinct noise levels were applied, yielding a total of 5000 simulated events evenly divided between high- and low-noise conditions. This approach ensured that the DAE was trained across realistic noise environments, thereby improving its robustness when applied to experimental data.

All events are preprocessed prior to training through baseline subtraction and normalization by their amplitude. For each pulse, the baseline is first estimated as the mean of the initial 100 samples and subtracted from the entire waveform to remove DC offsets. The resulting signal is then processed with a trapezoidal filter [23], and the amplitude is extracted as the maximum absolute value of the filtered output beyond the filter response region. The baseline-subtracted pulse is then normalized by this amplitude, resulting in a unit-amplitude, baseline-corrected signal. This standardized preprocessing pipeline is applied uniformly to both synthetic and experimental datasets to ensure robust and consistent inputs throughout model training and evaluation. It is worth noting that without this baseline subtraction and normalization, the DAE fails to accurately reconstruct pulse shapes.

After training on synthetic pulses, the DAE was then applied to real waveform data. To verify that the DAE

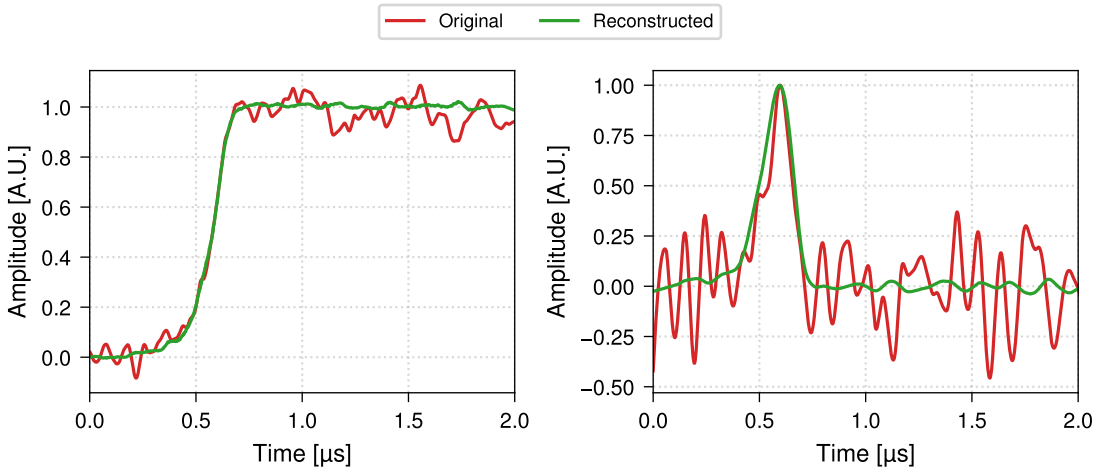

Figure 2: Effect of the denoising autoencoder on a real waveform (left) and on its derivative (right) for a low-energy pulse which corresponds to an energy of ~15 keV.

performed well on real data, we first checked that the reconstruction loss values of the DAE on synthetic and real data were consistent. As an example, the DAE effect on a normal waveform, which corresponds to an event of energy of 15 keV is shown in Figure 4. The reconstructed pulses produced by the DAE serve as inputs for the subsequent binary CNN classifier. Each event is represented by two input channels: (1) the normalized pulse, which is directly taken from the output of the DAE and requires no additional normalization, and (2) the normalized first derivative of the pulse, scaled to the range [0, 1]. By including both the pulse and its first derivative as separate input channels, the CNN can capture complex inter-relationships between the overall pulse shape and the subtle changes such as multi-site events. Signal events for training are defined as those that satisfy all of the following conditions:

1. Feature constraints: The rise time, full-width-at-half-maximum (FWHM) time, and L1 norm each fall within one standard deviation (1σ) of their respective total distributions. Rise time is the time interval for the pulse to increase from 10% to 90% of its maximum amplitude after baseline subtraction. FWHM time is the width of the pulse at half its maximum value, measured on both sides of the peak in the normalized first derivative space. L1 norm is the sum of absolute differences between the observed pulse and a reference pulse after baseline subtraction.

2. Peak count: The event contains exactly one peak in the normalized first derivative, as determined using

the `find_peaks` function from SciPy.

3. Labeling: As a further check all the waveforms are carefully labeled manually and assigned a signal label.

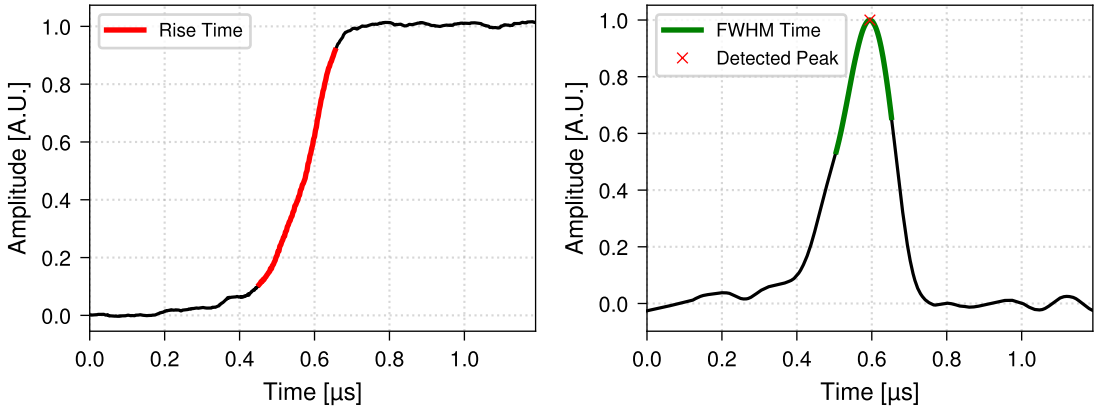

Figure 3: The rise time (left) is defined as the interval between 10% and 90% of the waveform amplitude (red). The FWHM time (right) is defined from the derivative of the waveform, with the FWHM interval highlighted in green.

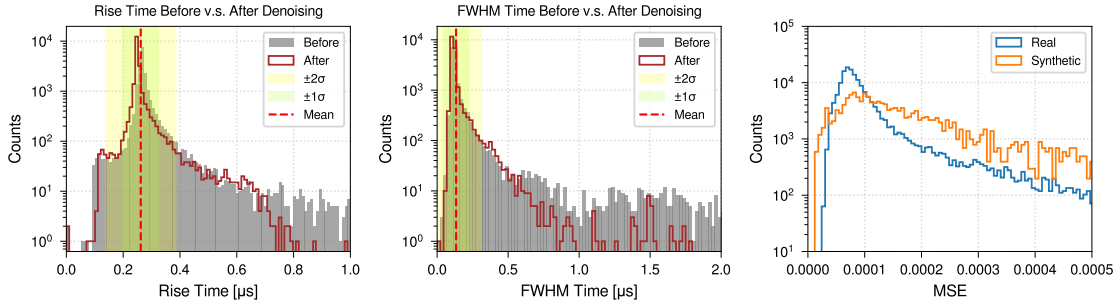

Figure 4: The rise time (left) is defined as the interval between 10% and 90% of the waveform amplitude (red). The FWHM time (right) is defined from the derivative of the waveform, with the FWHM interval highlighted in green.

This resulted in a dataset for supervised learning of waveforms. To train the CNN classifier, the dataset was split in training, validation, and testing with proportions 70%, 15% and 15%, respectively. The CNN model is composed of sequential 1D convolutional layers with increasing filter sizes (128,64,32) and decreasing kernel widths, each followed by batch normalization and max pooling to extract and condense features from the input. A fully connected dense layer interprets the extracted features, with a dropout layer included to mitigate overfitting. The final output layer uses a sigmoid activation function to produce a probability score for binary classification. The model is trained using the Adam optimizer with a learning rate of 10^{-5} and binary cross-entropy loss, and evaluated using accuracy, precision, and recall metrics. Early stopping of 10 epochs is employed to prevent overfitting and ensure optimal model weights. After training, the classifier assigns a probability to each event, representing the likelihood of it being a normal event. The classifier performance is evaluated using the receiver operating characteristic (ROC) curve and the F1-score, derived

from the true positive and false positive rates. The optimal classification threshold corresponds to the value that maximizes the F1-score. Figure 5 shows the ROC curve and the F1-score as a function of the threshold. The classifier achieved an AUC of 0.99 and an accuracy of 95% at the optimal threshold. The trained model is then applied to all reconstructed events, classifying them as normal or anomalous depending on whether their probability exceeds this threshold. Classifying events from extracted waveform features also gave good performance. However, computing these features in real time would be too demanding for live data acquisition. In contrast, the CNN classifier performs inference directly on the full waveform, allowing fast and efficient event classification during acquisition.

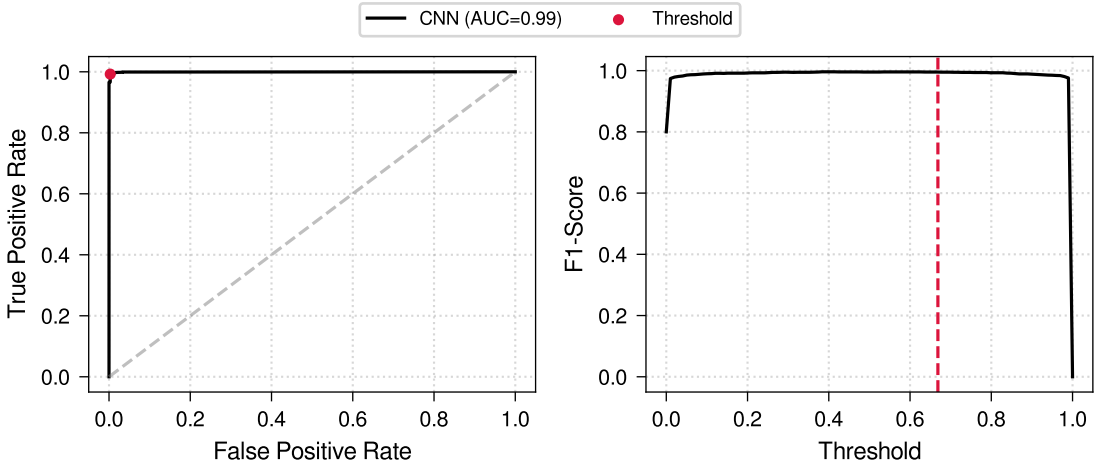

Figure 5: Performance of the CNN classifier applied to the denoising autoencoder output. Left: ROC curve with an AUC of 0.99, with the selected threshold marked in red. Right: accuracy and F1-score as a function of the classification threshold, with the chosen operating point indicated by the dashed red line.

3 Results and Discussion

Once the fiFigure-of-MeritFOM) which the spectrum. Once the training is complete, signal events are selected as those with a classification probability above the chosen threshold. An energy spectrum, fitted using a binned maximum likelihood method, is then constructed both before (Figure **??**) and after (Figure **??**) cleaning, using amplitudes extracted with a trapezoidal filter. Using the DAE-CNN workflow, the resolution (FWHM) at the ^{210}Pb peak and the energy threshold are determined to be approximately 1.47 keV and 11 keV, respectively. The calibration is performed using four peaks present in the spectrum, originating from the decay chains of ^{238}U: ^{210}Pb at 46 keV, ^{214}Pb at 295 keV and 352 keV, and ^{352}Bi at 609 keV, as shown in Figure **??**. Each spectrum is fitted with the following function:

$$f(x) = e^{a_1+b_1x}\,\frac{1}{2}\left[1+\mathrm{erf}\left(\frac{x-\mu_1}{\sigma_1}\right)\right] + e^{a_2+b_2x}\,\frac{1}{2}\left[1+\mathrm{erf}\left(\frac{x-\mu_2}{\sigma_2}\right)\right] + \sum_i A_i\,\exp\left(-\frac{(x-\mu_{g,i})^2}{2\sigma_{g,i}^2}\right).$$

The background is modeled as the sum of two error functions, where the first describes the exponential increase below 100 keV, and the second describes the exponential decrease above 100 keV. Each transition line is modeled with a Gaussian distribution. Without the DAE, events in the sub-15 keV range are dominated by electronic noise, making reliable analysis and event classification challenging. In contrast, the DAE effectively suppresses background noise and reconstructs the underlying signal, lowering the effective energy threshold to 11 keV. This directly addresses the experimental goal mentioned in Section **??**, where lowering the energy threshold is essential to enhance the sensitivity to rare processes. Furthermore, the use of the DAE

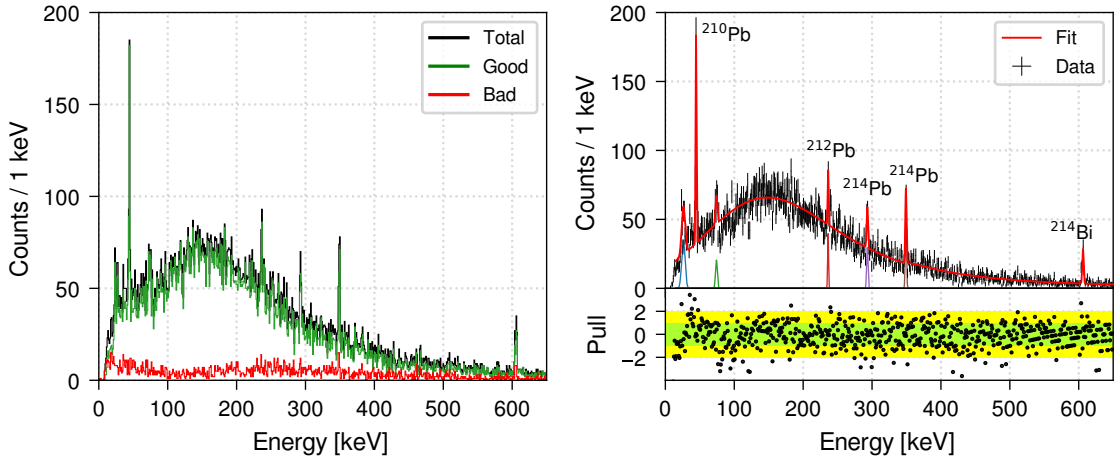

Figure 6: Left: measured spectra after machine-learning event selection, showing good (green), abnormal (red), and total (black) events. Right: BEGe spectrum (black) with the global fit (red) and individual Gaussian peak contributions (colored). The lower right panel shows the pull distribution with confidence intervals.

reduces the computational complexity of the subsequent CNN classification, as cleaner input waveforms allow for a simpler architecture without compromising classification performance. In addition, the DAE-preprocessing procedure allows for alternative analysis approaches, including traditional non-ML methods and feature-based ML techniques based on the extracted parameters from the denoised events. The ML-based approach yields a 14% improvement in the signal-to-background ratio compared to the baseline analysis, which is particularly impactful in the low-energy regime where background contributions are most significant.

Beyond immediate performance gains, this procedure can be further utilized as a scalable and transferable solution for low-background rare-event searches. The DAE-CNN workflow can be directly applied to ongoing datasets acquired with the BEGe detector in 2025 or similar experimental configurations, allowing the optimization of event selection strategies without requiring substantial retraining or hardware modifications. In addition, a Python package `vipbege` is provided alongside this work, allowing for the extraction of the features discussed here, as well as the generation of simulated waveforms both with and without noise, allowing its use for analysis in similar experimental configurations.

4 Conclusions

Data availability statement

Acknowledgments

We thank H. Schneider, L. Stohwasser, and D. Stückler from Stefan-Meyer-Institut for their fundamental contribution in designing and building the VIP-2 setup. We thank the Gran Sasso Underground Laboratory of INFN, INFN-LNGS, and its Director, Ezio Previtali, the LNGS staff, and the low radioactivity laboratory for the experimental activities dedicated to high-sensitivity tests of the Pauli exclusion principle.

Funding

This publication was made possible through the support of the INFN institute and Centro Ricerche Enrico Fermi Museo Storico della Fisica e Centro Studi e Ricerche “Enrico Fermi” Institute. We acknowledge the

support of grant 62099 from the John Templeton Foundation. The opinions expressed in this publication are those of the authors and do not necessarily reflect the views of the John Templeton Foundation. We acknowledge support from the Foundational Questions Institute and the Fetzer Franklin Fund, a donor-advised fund of the Silicon Valley Community Foundation (grant Nos. FQXi-RFP-CPW-2008 and FQXi-MGB-2011), and from the H2020 FET TEQ (grant No. 766900). We thank the Austrian Science Foundation (FWF), which supports the VIP-2 project with grants P25529-N20, project P 30635-N36 and W1252-N27 (doctoral college particles and interactions).

References

[1] Stephen L Adler et al. "Collapse Models with Non-White Noises". In: *Journal of Physics A: Mathematical and Theoretical* 40.50 (Nov. 2007), p. 15083. ISSN: 1751-8121. DOI: 10.1088/1751-8113/40/50/012.

[2] Angelo Bassi et al. "Models of Wave-Function Collapse, Underlying Theories, and Experimental Tests". In: *Reviews of Modern Physics* 85.2 (Apr. 2013), pp. 471–527. DOI: 10.1103/RevModPhys.85.471.

[3] W. Pauli. "The Connection Between Spin and Statistics". In: *Physical Review* 58.8 (Oct. 1940), pp. 716–722. DOI: 10.1103/PhysRev.58.716.

[4] Freeman J. Dyson et al. "Stability of Matter. I". In: *Journal of Mathematical Physics* 8.3 (Mar. 1967), pp. 423–434. ISSN: 0022-2488. DOI: 10.1063/1.1705209.

[5] Norman K. Glendenning. *Special and General Relativity: With Applications to White Dwarfs, Neutron Stars and Black Holes*. Springer Science & Business Media, Apr. 2010. ISBN: 978-0-387-47109-9.

[6] Raymond Frederick Streater et al. *PCT, Spin and Statistics, and All That*. Princeton University Press, 2000. ISBN: 978-0-691-07062-9.

[7] Erik Ramberg et al. "Experimental Limit on a Small Violation of the Pauli Principle". In: *Physics Letters B* 238.2 (Apr. 1990), pp. 438–441. ISSN: 0370-2693. DOI: 10.1016/0370-2693(90)91762-Z.

[8] G. C. Ghirardi. "Unified Dynamics for Microscopic and Macroscopic Systems". In: *Physical Review D* 34.2 (1986), pp. 470–491. DOI: 10.1103/PhysRevD.34.470.

[9] L. Diósi. "Gravitation and Quantum-Mechanical Localization of Macro-Objects". In: *Physics Letters A* 105.4 (Oct. 1984), pp. 199–202. ISSN: 0375-9601. DOI: 10.1016/0375-9601(84)90397-9.

[10] Roger Penrose. "On Gravity's Role in Quantum State Reduction". In: *General Relativity and Gravitation* 28.5 (May 1996), pp. 581–600. ISSN: 1572-9532. DOI: 10.1007/BF02105068.

[11] Kristian Piscicchia et al. "Optimization of a BEGe Detector Setup for Testing Quantum Foundations in the Underground LNGS Laboratory". In: *Condensed Matter* 9.2 (June 2024), p. 22. ISSN: 2410-3896. DOI: 10.3390/condmat9020022.

[12] G. Bellini et al. "Cosmic-Muon Flux and Annual Modulation in Borexino at 3800 m Water-Equivalent Depth". In: *Journal of Cosmology and Astroparticle Physics* 2012.05 (May 2012), p. 015. ISSN: 1475-7516. DOI: 10.1088/1475-7516/2012/05/015.

[13] XENON Collaboration et al. "First Dark Matter Search with Nuclear Recoils from the XENONnT Experiment". In: *Physical Review Letters* 131.4 (July 2023), p. 041003. DOI: 10.1103/PhysRevLett.131.041003.

[14] Majorana Collaboration et al. "Search for Neutrinoless Double-$\ensuremath{\beta}$ Decay in $^{76}\mathrm{Ge}$ with the Majorana Demonstrator". In: *Physical Review Letters* 120.13 (Mar. 2018), p. 132502. DOI: 10.1103/PhysRevLett.120.132502.

[15] GERDA Collaboration et al. “Final Results of GERDA on the Search for Neutrinoless Double-$\ensuremath{\beta}$ Decay”. In: *Physical Review Letters* 125.25 (Dec. 2020), p. 252502. DOI: 10.1103/PhysRevLett.125.252502.

[16] S. Bartalucci et al. “New Experimental Limit on the Pauli Exclusion Principle Violation by Electrons”. In: *Physics Letters B* 641.1 (Sept. 2006), pp. 18–22. ISSN: 0370-2693. DOI: 10.1016/j.physletb.2006.07.054.

[17] Fabrizio Napolitano et al. “Testing the Pauli Exclusion Principle with the VIP-2 Experiment”. In: *Symmetry* 14.5 (May 2022), p. 893. ISSN: 2073-8994. DOI: 10.3390/sym14050893.

[18] Simone Manti et al. “Testing the Pauli Exclusion Principle across the Periodic Table with the VIP-3 Experiment”. In: *Entropy* 26.9 (2024). ISSN: 1099-4300. DOI: 10.3390/e26090752.

[19] Pascal Vincent et al. “Stacked Denoising Autoencoders: Learning Useful Representations in a Deep Network with a Local Denoising Criterion”. In: *Journal of Machine Learning Research* 11.110 (2010), pp. 3371–3408. ISSN: 1533-7928.

[20] M. Agostini et al. “Characterization of a Broad Energy Germanium Detector and Application to Neutrinoless Double Beta Decay Search in 76Ge”. In: *Journal of Instrumentation* 6.04 (Apr. 2011), P04005. ISSN: 1748-0221. DOI: 10.1088/1748-0221/6/04/P04005.

[21] K.-H. Ackermann et al. “The Gerda Experiment for the Search of $0\nu\beta\beta$ Decay in 76Ge”. In: *The European Physical Journal C* 73.3 (Mar. 2013), p. 2330. ISSN: 1434-6052. DOI: 10.1140/epjc/s10052-013-2330-0.

[22] M. Agostini et al. “Pulse Shape Discrimination for Gerda Phase I Data”. In: *The European Physical Journal C* 73.10 (Oct. 2013), p. 2583. ISSN: 1434-6052. DOI: 10.1140/epjc/s10052-013-2583-7.

[23] Valentin T. Jordanov et al. “Digital Synthesis of Pulse Shapes in Real Time for High Resolution Radiation Spectroscopy”. In: *Nuclear Instruments and Methods in Physics Research Section A: Accelerators, Spectrometers, Detectors and Associated Equipment* 345.2 (June 1994), pp. 337–345. ISSN: 0168-9002. DOI: 10.1016/0168-9002(94)91011-1.